

Article

Formation Control for UAV-USVs Heterogeneous System with Collision Avoidance Performance

Yuyang Huang ¹ , Wei Li ¹ , Jun Ning ^{1,*}  and Zhihui Li ²

¹ College of Navigation, Dalian Maritime University, Dalian 116026, China; huangyuyang@dmlu.edu.cn (Y.H.); li_wei@dmlu.edu.cn (W.L.)

² College of Information Technology, Jilin Normal University, Siping 136000, China; lizhihui1650@163.com

* Correspondence: junning@dmlu.edu.cn

Abstract: This paper investigates the cooperative formation trajectory tracking problem for heterogeneous unmanned aerial vehicle (UAV) and multiple unmanned surface vessel (USV) systems with collision avoidance performance. Firstly, a formation control protocol based on extended state observer (ESO) is proposed to ensure that the UAV and the USVs track the target trajectory simultaneously in the XY plane. Then, the collision avoidance control strategy of USV formation based on artificial potential field (APF) theory is designed. Specifically, the APF method is improved by reconstructing the repulsive potential field to make the collision avoidance action of USVs more in line with the requirements of International Regulations for Preventing Collisions at Sea (COLREGs). Following that, an altitude controller for the UAV is proposed to maintain the cooperative formation of the heterogeneous systems. Based on the input-to-state stability, the stability of the proposed control structure is proven, and all the signals in the closed-loop system are ultimately bounded. Finally, a simulation study is provided to show the efficacy of the proposed strategy.

Keywords: heterogeneous formation control system; UAV-USVs; extended state observer; collision avoidance; artificial potential field method



Citation: Huang, Y.; Li, W.; Ning, J.; Li, Z. Formation Control for UAV-USVs Heterogeneous System with Collision Avoidance Performance. *J. Mar. Sci. Eng.* **2023**, *11*, 2332. <https://doi.org/10.3390/jmse11122332>

Academic Editor: Weicheng Cui

Received: 9 October 2023

Revised: 24 November 2023

Accepted: 7 December 2023

Published: 10 December 2023



Copyright: © 2023 by the authors. Licensee MDPI, Basel, Switzerland. This article is an open access article distributed under the terms and conditions of the Creative Commons Attribution (CC BY) license (<https://creativecommons.org/licenses/by/4.0/>).

1. Introduction

In the past few years, unmanned systems have gained significant prominence in the realm of industrial advancement, attributed to their diverse usage in areas such as reconnaissance [1,2], marine pollution tracking [3,4], and advanced traffic management [5,6]. These systems principally encompass unmanned aerial vehicles (UAVs), unmanned ground vehicles (UGVs), unmanned surface vehicles (USVs), and autonomous underwater vehicles (AUVs) [7,8]. Although each unmanned system can handle tasks, its capacity limits its ability to deal with more complex tasks. Therefore, a homogeneous or heterogeneous system is more effective than a single unmanned system in completing intricate tasks [9–11].

The development of USV has been widely employed in ocean engineering due to its benefits, which include increased loading capacity, more convenience, and cheaper mission costs [12,13]. However, finding the rescue target in rescue missions and maritime searches is difficult owing to the restricted observation range of USVs [14,15]. Fortunately, incorporating UAVs into USV systems to construct heterogeneous multi-agent systems can compensate for this shortcoming [16,17]. A USV usually boosts its capacity to operate at sea by using the UAV's flexibility and utilizing the powerful target search ability while simultaneously widening the communication range of the sea between USVs, therefore, the heterogeneous systems extend the effective working area [18,19]. As a result, it is critical to investigate the formation challenges of a heterogeneous system, which has primarily engineering importance.

For the cooperative tracking control problem of UAVs and USVs, many research results have been addressed, among which typical control methods include the leader following

method [20], virtual structure method [21], behavior-based approach [22], and model prediction method [23]. In [24], a series of coordinate transformations have been developed to convert the tracking error dynamics of a marine aerial-surface heterogeneous system into translation-rotation cascade forms. This eliminates variability between the UAV and the USV in terms of both translation and rotation dynamics. In [25], the research proposes an adaptive fault-tolerant time-varying formation control scheme. This scheme is particularly tailored to address challenges posed by actuator failures, parameter uncertainties, and external disturbances within the framework of a directed communication topology.

In the area of cooperative control of heterogeneous formations of UAVs and USVs, a globally applicable fixed-duration adaptive neural network is designed in [18] that employs a nonsingular rapid terminal sliding approach for formation control. This protocol is engineered to accurately follow a specified trajectory and achieve a predefined formation arrangement within a set timeframe, effectively addressing a range of uncertainties. This is accomplished by harnessing the combined strengths of adaptive methodologies and Radial Basis Function (RBF) neural networks. In [26], the research proposes a velocity estimation-based control strategy that comprises a distributed observer for estimating each vehicle's reference velocity. In [23], a distributed model predictive control algorithm tailored for heterogeneous systems is presented, characterized by a directed topological structure.

It is worth noting that the above research results tend to focus on the establishment of air-sea cooperation and the realization of trajectory tracking without considering the problem of collision avoidance [27,28]. During the mission, a minimum safe distance has to be maintained between any two unmanned systems to prevent collisions and to avoid damage to the overall performance of the search and rescue cooperative mission. Therefore, another key issue for the heterogeneous formation system is collision avoidance. Collision avoidance includes not only avoiding collisions between unmanned systems or between unmanned systems and other individuals but also avoiding collisions between unmanned systems and obstacles. Collision avoidance can be further divided into static collision avoidance based on sensor information and dynamic collision avoidance based on an unknown environment. Collision avoidance between aerial vehicles and obstacles can be divided into two ways: overall collision avoidance and changing formation collision avoidance.

There are relatively few research results on the cooperative formation control of heterogeneous systems with collision avoidance and obstacle avoidance. To avoid collision between ships, [29,30] propose an unmanned ship formation control method based on guaranteed performance, but the collision avoidance of obstacles is not addressed. For the collision avoidance problem between UAVs with static and dynamic obstacles, a cooperative controller for multiple unmanned ships based on artificial potential function is proposed in [12,31], while in the area of cooperative collision avoidance and obstacle avoidance for heterogeneous systems, research results are more limited. In [32], a distributed heterogeneous cooperative tracking control approach is proposed based on the leader-following method, and the artificial potential field (APF) algorithm is used to construct a control strategy with a collision avoidance mechanism. However, the research results between vehicles ignore the nautical engineering practice and poorly consider the COLREGs.

Based on the preceding analysis, this paper investigates the cooperative formation trajectory tracking problem for UAV-USV heterogeneous systems with model uncertainty and external disturbances. To solve this problem, a formation control protocol based on extended state observer (ESO) is proposed to ensure that UAV and USV track the target trajectory simultaneously. The collision avoidance control strategy of USV formation based on improved APF theory is designed. The collision avoidance problem between multiple USV formations formed under UAV coordination is solved by innovatively introducing the ship encounter situation and danger evaluation index into the artificial potential field. The key contributions can be summarized as follows:

- (1) Compared with the existing results in [12,29–31], which only study the cooperative trajectory tracking problem of UAV and USV heterogeneous systems, this paper

explores the collision avoidance protocol for USV formation under UAV cooperation with navigation practice.

- (2) Compared with the existing results in [18,25,26,32], which estimate that the system’s indeterminate terms rely on RBF neural networks and fuzzy logic, etc., this paper employs ESO to realize the accurate compensation of uncertainties and external disturbances in heterogeneous systems.
- (3) Compared with the existing results in [31–37], this paper innovatively introduces the ship encounter situation and danger evaluation index into the APF approach, and the improved APF method for heterogeneous cooperative control collision avoidance decision is more in line with the navigation practice.

The organization of this paper is structured as follows. Section 2 formulates the problem. Section 3 expounds on the controller design and the closed-loop system stability analysis. Section 4 demonstrates the simulation illustrations. Section 5 concludes this paper.

2. Preliminaries and Problem Statement

2.1. Problem Formulation

Consider the heterogeneous systems consisting of one UAV and N USVs. First, the dynamic models of the UAV and N USVs are presented. They are used to illustrate a unified dynamic model for the heterogeneous system. For ease of use, let $\Pi = \{1, 2, \dots, N\}$. According to the results in [38], the dynamic model of the quadrotor UAV can be described as

$$\begin{cases} \ddot{p}_{ax} = (\sin \phi_a \sin \psi_a + \cos \phi_a \sin \theta_a \cos \psi_a) \frac{u_{ap}}{m_a} - \frac{d_{ax}\dot{p}_{ax}}{m_a} + \Delta_{ax}, \\ \ddot{p}_{ay} = (\sin \phi_a \cos \psi_a + \cos \phi_a \sin \theta_a \sin \psi_a) \frac{u_{ap}}{m_a} - \frac{d_{ay}\dot{p}_{ay}}{m_a} + \Delta_{ay}, \\ \ddot{p}_{az} = (\cos \theta_a \cos \phi_a) \frac{u_{ap}}{m_a} - \frac{d_{az}\dot{p}_{az}}{m_a} - g_a + \Delta_{az}, \end{cases} \quad (1)$$

$$\begin{cases} \ddot{\phi}_a = \dot{\theta}_a \dot{\psi}_a \frac{J_{ay} - J_{az}}{J_{ax}} - \frac{J_{ar}}{J_{ax}} \dot{\theta}_a \dot{\bar{d}}_a + \frac{\tau_{a\phi}}{J_{ax}} - \frac{d_{a\phi}\dot{\phi}_a}{J_{ax}}, \\ \ddot{\theta}_a = \dot{\phi}_a \dot{\psi}_a \frac{J_{az} - J_{ax}}{J_{ay}} - \frac{J_{ar}}{J_{ay}} \dot{\phi}_a \dot{\bar{d}}_a + \frac{\tau_{a\theta}}{J_{ay}} - \frac{d_{a\theta}\dot{\theta}_a}{J_{ay}}, \\ \ddot{\psi}_a = \dot{\phi}_a \dot{\theta}_a \frac{J_{ax} - J_{ay}}{J_{az}} + \frac{\tau_{a\psi}}{J_{az}} - \frac{d_{a\psi}\dot{\psi}_a}{J_{az}}, \end{cases} \quad (2)$$

where $[\phi_a, \theta_a, \psi_a]^T$ is the attitude state, $[p_{ax}, p_{ay}, p_{az}]^T$ is the position state, $\tau_{a\phi}, \tau_{a\theta}, \tau_{a\psi}$ are the three control torques, u_{ap} is the control thrust, g_a is the gravitational acceleration, m_a denotes the mass, \bar{d}_a is the overall residual rotor angle, J_{ax}, J_{ay}, J_{az} represent the moments of the inertia, $d_{ax}, d_{ay}, d_{az}, d_{a\phi}, d_{a\theta}, d_{a\psi}$ represent the translational drag coefficients, $\Delta_{ax}, \Delta_{ay}, \Delta_{az}$ are the external disturbances encountered, and J_{ar} denotes the moment of rotor’s inertia.

Inspired by the results in [25], the UAV’s rotational dynamics can be stabilized separately. Therefore, in light of external disturbances and parametric uncertainties, the UAV model (1) is redefined in the following manner

$$\ddot{p}_a = g_a u_a + f_a + \Delta_a \quad (3)$$

where $p_a = [p_{ax}, p_{ay}, p_{az}]^T$ is the position, $f_a = [-d_{ax}\dot{p}_{ax}/m_a, -d_{ay}\dot{p}_{ay}/m_a, -d_{az}\dot{p}_{az}/m_a - g_a]^T$, $g_a = \text{diag}\{1/m_a, 1/m_a, 1/m_a\}$, $\Delta_a = [\Delta_{ax}, \Delta_{ay}, \Delta_{az}]^T$, $u_a = [u_{ax}, u_{ay}, u_{az}]^T$ denotes the new control signal which is given as [39]

$$\begin{cases} u_{ax} = (\sin \phi_a \sin \psi_a + \cos \phi_a \sin \theta_a \cos \psi_a) u_p \\ u_{ay} = (\sin \phi_a \cos \psi_a + \cos \phi_a \sin \theta_a \sin \psi_a) u_p \\ u_{az} = (\cos \theta_a \cos \phi_a) u_p \end{cases}$$

In the horizontal plane, the i -th ($i \in \Pi$) USV’s kinematic and dynamic equations are described as [40]

$$\begin{cases} \dot{x}_{bi} = \mu_{bi} \cos \psi_{bi} - v_{bi} \sin \psi_{bi}, \\ \dot{y}_{bi} = \mu_{bi} \sin \psi_{bi} + v_{bi} \cos \psi_{bi}, \\ \dot{\psi}_{bi} = r_{bi} \end{cases} \quad (4)$$

$$\begin{cases} \dot{\mu}_{bi} = f_{\mu bi}(\alpha_i) + \frac{1}{m_{\mu bi}} (\tau_{\mu bi}^f + w_{\mu bi}), \\ \dot{v}_{bi} = f_{v bi}(\alpha_i) + \frac{1}{m_{v bi}} w_{v bi} \\ \dot{r}_{bi} = f_{r bi}(\alpha_i) + \frac{1}{m_{r bi}} (\tau_{r bi}^f + w_{r bi}) \end{cases} \quad (5)$$

and

$$\begin{cases} f_{\mu bi}(\alpha_i) = \frac{1}{m_{\mu bi}} (m_{v bi} v_{bi} r_{bi} - d_{\mu bi} \mu_{bi} - d_{\mu bi 1} |\mu_{bi}| \mu_{bi}) \\ f_{v bi}(\alpha_i) = \frac{1}{m_{v bi}} (-m_{\mu bi} \mu_{bi} r_{bi} - d_{v bi} v_{bi} - d_{v bi 1} |v_{bi}| v_{bi}), \\ f_{r bi}(\alpha_i) = \frac{1}{m_{r bi}} ((m_{\mu bi} - m_{v bi}) \mu_{bi} v_{bi} - d_{r bi} r_{bi} - d_{r bi 1} |r_{bi}| r_{bi}), \end{cases} \quad (6)$$

where ψ_{bi} denotes the yaw angle; (x_{bi}, y_{bi}) denotes the position; $\alpha_i = [\mu_{bi}, v_{bi}, r_{bi}]^T$ denote the surge, sway, and yaw velocity, respectively; $m_{\mu bi}, m_{v bi}, m_{r bi}$ represent the inertial mass; $f_{\mu bi}(\alpha_i), f_{v bi}(\alpha_i), f_{r bi}(\alpha_i)$ denote the nonlinear dynamics consisting of Coriolis forces and the unmodeled hydrodynamics; $w_{\mu bi}, w_{v bi}, w_{r bi}$ represent the bounded disturbances; and $\tau_{\mu bi}^f$ and $\tau_{r bi}^f$ represent the surge force and the yaw moment.

Because the USVs' motion model given in (4) and (5) is underactuated, a hand position technique is employed to compensate. The USVs' front point (p_{bix}, p_{biy}) is defined as the hand point, which can be expressed as

$$\begin{cases} p_{bix} = x_{bi} + L_{bi} \cos \psi_{bi} \\ p_{biy} = y_{bi} + L_{bi} \sin \psi_{bi} \end{cases} \quad (7)$$

where L_{bi} denotes the distance between the new defined hand point (p_{bix}, p_{biy}) and the actual position (x_{bi}, y_{bi}) , which is depicted in Figure 1.

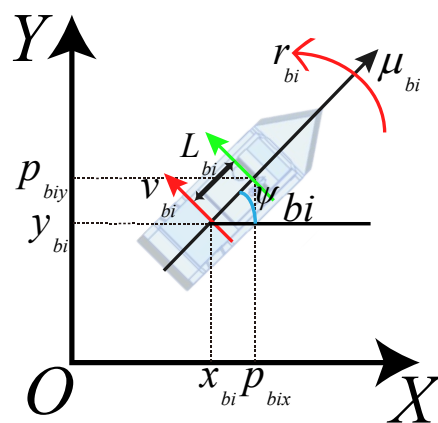


Figure 1. The kinematic model of USV.

The second derivative of (7) yields the following result

$$\begin{cases} \ddot{p}_{bix} = \dot{\mu}_{bi} \cos \psi_{bi} - (\dot{v}_{bi} + L_{bi}\dot{r}_{bi}) \sin \psi_{bi} - \mu_{si}r_{bi} \sin \psi_{bi} \\ \quad - (v_{bi}r_{bi} + L_{bi}r_{bi}^2) \cos \psi_{bi} \\ \ddot{p}_{biy} = \dot{\mu}_{bi} \sin \psi_{bi} - (\dot{v}_{bi} + L_{bi}\dot{r}_{bi}) \cos \psi_{bi} + \mu_{si}r_{bi} \cos \psi_{bi} \\ \quad - (v_{bi}r_{bi} + L_{bi}r_{bi}^2) \sin \psi_{bi} \end{cases} \quad (8)$$

Substituting (6) into (8) gives that

$$\begin{cases} \ddot{p}_{bix} = f_{bix}(\beta) + \frac{\cos \psi_{bi}}{m_{\mu bi}} \tau_{\mu}^f - \frac{L_{bi} \sin \psi_{bi}}{m_{rbi}} \tau_r^f + w_{bix} \\ \ddot{p}_{biy} = f_{biy}(\beta) + \frac{\sin \psi_{bi}}{m_{\mu bi}} \tau_{\mu}^f + \frac{L_{bi} \cos \psi_{bi}}{m_{rbi}} \tau_r^f + w_{biy} \end{cases} \quad (9)$$

where

$$\begin{cases} f_{bix}(\beta) = f_{\mu}(\alpha) \cos \psi_{bi} - (f_v(\alpha) + L_{bi}f_r(\alpha)) \sin \psi_{bi} \\ \quad - \mu_{bi}r_{bi} \sin \psi_{bi} - (v_{bi}r_{bi} + L_{bi}r_{bi}^2) \cos \psi_{bi} \\ f_{biy}(\beta) = f_{\mu}(\alpha) \sin \psi_{bi} + (f_v(\alpha) + L_{bi}f_r(\alpha)) \cos \psi_{bi} \\ \quad + \mu_{bi}r_{bi} \cos \psi_{bi} - (v_{bi}r_{bi} + L_{bi}r_{bi}^2) \sin \psi_{bi} \end{cases}$$

$$\begin{cases} w_{bix}(\beta) = \frac{w_{\mu bi}}{m_{\mu bi}} \cos \psi_{bi} - \left(\frac{w_{vbi}}{m_{\mu bi}} + \frac{L_{bi}w_{rbi}}{m_{rbi}} \right) \sin \psi_{bi} \\ w_{biy}(\beta) = \frac{w_{\mu bi}}{m_{\mu bi}} \sin \psi_{bi} + \left(\frac{w_{vbi}}{m_{\mu bi}} + \frac{L_{bi}w_{rbi}}{m_{rbi}} \right) \cos \psi_{bi} \end{cases}$$

with $\beta = [\mu_{bi}, v_{bi}, r_{bi}, \psi_{bi}]^T$.

Based on (9), the i -th USV position dynamics can be described as

$$\dot{p}_{bi} = f_{bixy} + \Omega_{bi}(\psi_{bi})\omega_{bi}u_{bi} + w_{bixy} \quad (10)$$

where $p_{bi} = [p_{bix}, p_{biy}]^T$ is the i -th USV position, $f_{bixy} = [f_{bix}, f_{biy}]^T$, $\Omega_{bi}(\psi_{bi}) = [\cos \psi_{bi}, -\sin \psi_{bi}; \sin \psi_{bi}, \cos \psi_{bi}]$, $u_{bi} = [\tau_{\mu}, \tau_r]^T$, $\omega_{bi} = \text{diag}\{1/m_{\mu bi}, L_{bi}/m_{rbi}\}$, $w_{bixy} = [w_{bix}, w_{biy}]^T$.

Combining (3) and (10), the unified model of the heterogeneous systems can be described as

$$\begin{cases} \dot{x}_{i1} = x_{i2} \\ \dot{x}_{i2} = F_{xi} + G_{xi}u_{xi} + \Delta_{xi} \end{cases} \quad (11)$$

When (11) represents the UAV model. Where $x_{i1} = [p_{ax}, p_{ay}]^T = x_{a1} \in R^2$, $x_{i2} = [\dot{p}_{ax}, \dot{p}_{ay}]^T = x_{a2} \in R^2$, $F_{xi} = F_{axy} = [-d_x \dot{p}_{ax}/m_a, -d_y \dot{p}_{ay}/m_a]^T$, $G_{xi} = G_{axy} = \text{diag}\{1/m_a, 1/m_a\}$, $\Delta_{xi} = \Delta_{axy} = [\Delta_{ax}, \Delta_{ay}]^T$, $u_{xi} = u_{axy} = [u_{ax}, u_{ay}]^T$.

When (11) represents the USV model. Where $x_{i1} = [p_{bix}, p_{biy}]^T = x_{bi1} \in R^2$, $x_{i2} = [\dot{p}_{bix}, \dot{p}_{biy}]^T = x_{bi2} \in R^2$, $F_{xi} = f_{bixy} = [f_{bix}, f_{biy}]^T$, $G_{xi} = \Omega_{bi}(\psi_{bi})\omega_{bi}$, $\Delta_{xi} = w_{bixy} = [w_{bix}, w_{biy}]^T$, $u_{xi} = u_{bi} = [\tau_{\mu}, \tau_r]^T$.

The virtual leader is defined and its motion model is described as follows

$$\begin{cases} \dot{x}_{l1} = x_{l2} \\ \dot{x}_{l2} = F_l \end{cases} \quad (12)$$

where $x_{l1} \in R^2, x_{l2} \in R^2$ denote the position and velocity state vectors, respectively. $F_l \in R^2$ is a smooth unknown nonlinear function.

Define the system's error variable as

$$\begin{cases} \bar{x}_{i1} = x_{i1} - x_{l1} - \delta_i \\ \bar{x}_{i2} = x_{i2} - x_{l2} \end{cases} \tag{13}$$

where $\delta_i \in R^2$ represents the desired relative position vector between i -th of the agent of the heterogeneous systems and the virtual leader.

Assumption 1. The aerodynamic drag coefficients d_{ix}, d_{iy} , and d_{iz} are bounded and unknown. The unknown nonlinear function F_l is bounded. Then, there exists a positive constant α_l such that $F_l < \alpha_l$.

Assumption 2. The quadrotor UAV experiences external perturbations $\Delta_{ax}, \Delta_{ay}, \Delta_{az}$, which are confined within certain bounds, fulfilling the conditions $\|\Delta_{ax}\| \leq \bar{\Delta}_{ax}, \|\Delta_{ay}\| \leq \bar{\Delta}_{ay}, \|\Delta_{az}\| \leq \bar{\Delta}_{az}$. Here, $\bar{\Delta}_{ax}, \bar{\Delta}_{ay}$, and $\bar{\Delta}_{az}$ represent unknown positive constants. The USV experiences external disturbances $w_{\mu bi}, w_{v bi}, w_{r bi}$ which are confined within certain limits, fulfilling the conditions $\|w_{\mu bi}\| \leq \bar{w}_{\mu bi}, \|w_{v bi}\| \leq \bar{w}_{v bi}, \|w_{r bi}\| \leq \bar{w}_{r bi}$. In this context, $\bar{w}_{\mu bi}, \bar{w}_{v bi}$, and $\bar{w}_{r bi}$ signify unknown positive constants.

Assumption 3. The velocity and acceleration of the agent and the virtual leader are bounded, and they satisfy $v_l \neq 0, v_i \neq 0$.

Assumption 4. G_{xi} is a symmetric matrix and its eigenvalues $\lambda_1, \lambda_2, \dots, \lambda_m$ are satisfied such that $0 < \vartheta_i < \lambda_1 < \lambda_2 \dots < \lambda_m < \infty$, where ϑ_i is a positive constant.

Theorem 1 ([41]). For any point in time, the function $V(t)$ is continuous and positive, with its initial state being within limits. Given that the inequality $\dot{V}(t) \leq -\gamma V(t) + \mu$ is satisfied, where $\gamma > 0$ and $\mu > 0$, it can be deduced that

$$V(t) \leq \frac{\mu}{\gamma}(1 - e^{-\gamma t}) + V(0)e^{-\gamma t}.$$

Theorem 2 ([42]). At all moments, the function $S(t)$ remains positive and continuous, with its initial condition $S(0)$ being constrained. Should the condition $\dot{S}(t) > qS(t)$ be valid for $t - t_0 \geq 0$ with $q > 0$, it leads to the inference that

$$S(t) > e^{q(t-t_0)} S(t_0).$$

2.2. Algebraic Graph Theory

$G = (V_g, \varepsilon_g, A_g)$ is an undirected graph in this paper, with $V_g = \{v_1, v_2, \dots, v_n\}$ being the node-set, $\varepsilon_g \subseteq V_g \times V_g$ being the edge set, and $A_g = [a_{ij}]$ being the adjacency matrix, of which all the elements are non-negative. The adjacency matrix A_g depicts the effectiveness of communication from agent j to agent i , where a_{ij} denotes the communication weight corresponding to the edge, and diagonal element $a_{ii} = 0, a_{ij} > 0$. As an undirected graph, the adjacency element $a_{ij} = a_{ji}$ must be guaranteed to be satisfied. If any pair of unique nodes can be connected by an undirected path, then the graph is connected. The Laplacian matrix $L_g = [l_{ij}] \in R^{n \times n}$ is defined as follows

$$L_g = D_g - A_g$$

where $D_g = \text{diag}\{d_1, d_2, \dots, d_n\}, d_i = \sum_{j=1}^n a_{ij}$ and $i = 1, 2, \dots, n$. Defining the leader adjacency weight matrix as $B_g = \text{diag}\{b_1, b_2, \dots, b_n\}$, where $b_i > 0$, indicates an exchange of

information between agent i and the leader, otherwise, $b_i = 0, i = 1, 2, \dots, n$. It is presupposed that there is always at least one agent linked to the leader and $b_1 + b_2 + \dots + b_n > 0$.

Theorem 3 ([43]). G must be irreducible for the graph to be linked.

Theorem 4 ([43]). $\tilde{L}_g = L_g + B_g = \begin{bmatrix} l_{11} + b_1 & \dots & l_{1n} \\ \vdots & \ddots & \vdots \\ l_{n1} & \dots & l_{nn} + b_n \end{bmatrix}$ are positive, where B_g is the leader adjacency weight matrix if the Laplacian matrix L_g of the undirected graph G is irreducible.

2.3. Improved Artificial Potential Field and Virtual Repulsion

The essential concept of the APF technique is that each agent is viewed as a high-potential field for the control objective of collision avoidance. Any agent that is close to the others will be repelled from their potential fields by the repulsive force. Specifically, the APF method has fewer design parameters and a significantly simpler controller architecture. Some results regard the agent as a particle, which makes collision avoidance issues impractical. In actuality, the domain of agents should be considered during an encounter situation. As illustrated in Figure 2, the domain of USV can be defined as three concentric circles with unequal radii.

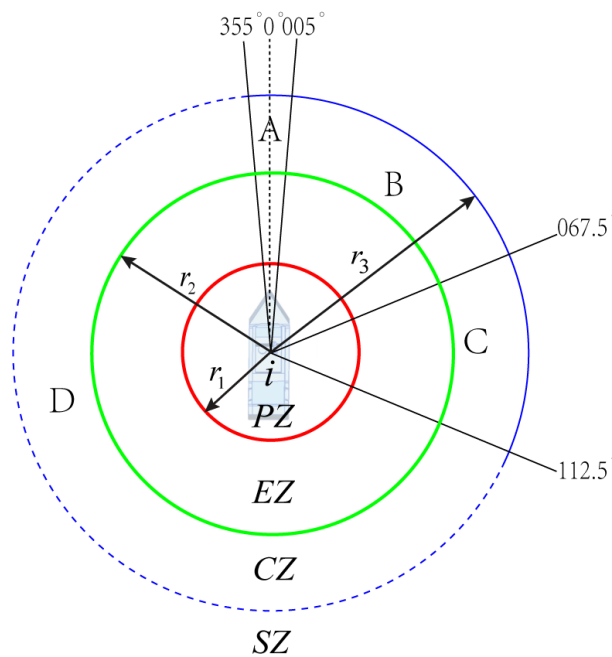


Figure 2. Repulsive potential field partition.

As is shown in Figure 2, the repulsive force field is separated into the following four areas. The area outside the first circular area is defined as the Safe Zone, where d_{ij} is greater than the detection distance r_3 of the potential field, there is no repulsive force in this area. The area inside the first circular area and outside the second circular is defined as the Negotiation Collision Avoidance Zone, where the distance d_{ij} is larger than r_2 and less than or equal to r_3 . If the incoming ship is in zones A, B, or C in the area, the i -th USV is a giving-way vessel or has the same avoidance responsibility, and the i -th USV should take collision avoidance actions to avoid the collision. If the incoming ship is in zone D, the i -th USV is a stand-on vessel. The area inside the second circular area and outside the third circular area is defined as the Emergency Collision Avoidance Zone, where the distance d_{ij} is larger than r_1 and less than or equal to r_2 . In the area where the distance between the other ship and the i -th USV is larger than and less than r_2 , the i -th USV should perform emergency collision avoidance actions that can momentarily violate the COLREGs.

The area within the third circular area is defined as the Prohibited Zone, which is shown by the red circular limit with radius r_1 in Figure 2. All other USVs are prohibited from entering this area.

Where $d_{ij} = x_i - x_j$ represents the relative position variable between the i -th USV and the incoming j -th USV, $\|d_{ij}\|$ represents the distance variable, and r_3 is the collision hazard detection distance, we conclude that the j -th USV is defined as a collision avoidance neighbor Π^c of the i -th USV. Once its collision avoidance neighbor Π^c holds $\|d_{ij}\| = \|x_i - x_j\| \leq 2r_1$, it can be defined that the systems have been collided.

When the judgment condition $355^\circ \leq T_r < 360^\circ$ or $0^\circ \leq T_r < 67.5^\circ$, $r_2 < d_{ij} \leq r_3$ are met, the incoming j -th USV is in Zone A and Zone B. Meanwhile, when the judgment condition $67.5^\circ < T_r \leq 112.5^\circ$, $r_2 < d_{ij} \leq r_3$ are met, the incoming j -th USV is in Zone C. The i -th USV is a give-way ship. According to the COLREGs, it should turn right to give way. The repulsive force field is shown as follows [34]:

$$\varphi_{ij}(p, v) = \eta_d R_j \left(e^{\theta_m - \theta} - 1 \right) \left(\frac{1}{d_{ij} - r_2} - \frac{1}{\rho_0} \right) \tag{14}$$

when the judgment condition $r_1 < d_{ij} \leq r_2$ is met, the i -th USV needs emergency collision avoidance. The repulsive force field is shown as follows:

$$\varphi_{ij}(p, v) = \eta_d R_j \left[\left(\frac{1}{d_{ij} - r_1} - \frac{1}{\rho_0} \right)^2 + (\|v_{ot}\| \cos \theta)^2 \right] \tag{15}$$

When $d_{ij} > r_2$ or the incoming j -th USV is in Zone D, the repulsion field is not defined, that is, the repulsion is zero.

Where p and v are the position and speed, T_r denotes the relative position of the incoming j -th USV and the i -th USV, η_d is the positive scaling factor for the USVs, R_j is the radius of the puffing circle of the other ship, ρ_0 denotes the repulsive potential field's influence radius of other ships, θ_m is the angle between the maximum relative position line, θ is the angle between p_{ot} , v_{ot} , p_{ot} denotes the relative position line of the i -th USV and other ships, and v_{ot} denotes the relative velocity.

The virtual repulsive force f_{ij}^{ca} is defined as the negative gradient of the repulsive potential function $\varphi_{ij}(p, v)$ as follows:

$$f_{ij}^{ca} = -\nabla_{(p,v)} \varphi_{ij}(p, v) \tag{16}$$

where $-\nabla_{(p,v)}$ represents a negative gradient along p and v .

The total virtual repulsive force term of the whole systems is induced from (14)–(16) as follows:

$$u_i^{ca} = -\frac{\omega_i}{\vartheta_i} \sum_{j \in \Pi^c} \nabla_{(p,v)} \varphi_{ij}(p, v) \tag{17}$$

where ω_i denotes the positive gain parameter and ϑ_i is a positive constant.

3. Main Results

This section introduces a formation control protocol utilizing an extended state observer, aimed at guiding heterogeneous systems to follow a predefined trajectory in the XY plane, accounting for model uncertainties and external disturbances. Subsequently, a decentralized formation controller is developed to manage the height-tracking control of the UAV along the Z axis.

3.1. Controller Design Based on ESO

Rewrite (11) as

$$\begin{cases} \dot{x}_{i1} = x_{i2} \\ \dot{x}_{i2} = F_i + G_{xi}u_{xi} \end{cases} \tag{18}$$

where $F_i = [F_{Ti}, F_{Li}]^T = F_{xi} + \Delta_{xi}$, F_{Ti} and F_{Li} denote the transverse and longitudinal orientation of F_i and F_1 denotes the sum of the nonlinear unknown term and the external disturbance encountered of the UAV. F_2, F_3, F_4, F_5 denote the sum of the nonlinear unknown term and the external disturbance encountered by different USVs, respectively.

For the purpose of approximating F_i , the design of an extended state observer has been formulated as follows

$$\begin{cases} \dot{\hat{x}}_{i1} = \hat{x}_{i2} + \frac{\alpha_{i1}}{\varepsilon_i} k_{xi} \\ \dot{\hat{x}}_{i2} = G_{xi}u_{xi} + \hat{F}_i + \frac{\alpha_{i2}}{\varepsilon_i^2} k_{xi} \\ \dot{\hat{F}}_i = \frac{\alpha_{i3}}{\varepsilon_i^3} k_{xi} \end{cases} \tag{19}$$

where $\hat{x}_{i1}, \hat{x}_{i2}, \hat{F}_i$ represent the observer state, $\varepsilon_i > 0, \alpha_{i1} \in \mathbb{R}, \alpha_{i2} \in \mathbb{R}, \alpha_{i3} \in \mathbb{R}$ are positive constants, $k_{xi} = x_{i1} - \hat{x}_{i1}$. According to (19), we have

$$\begin{cases} \dot{\tilde{x}}_{i1} = \tilde{x}_{i2} + \frac{\alpha_{i1}}{\varepsilon_i} k_{xi} \\ \dot{\tilde{x}}_{i2} = \tilde{F}_i + \frac{\alpha_{i2}}{\varepsilon_i^2} k_{xi} \\ \dot{\tilde{F}}_i = \frac{\alpha_{i3}}{\varepsilon_i^3} k_{xi} - \dot{\tilde{F}}_i \end{cases} \tag{20}$$

where $\tilde{x}_{i1} = \hat{x}_{i1} - x_{i1}$ is the ESO estimation error.

Define η_i as

$$\eta_i = [\eta_{i1} \quad \eta_{i2} \quad \eta_{i3}]^T$$

where

$$\eta_{i1} = \frac{x_{i1} - \hat{x}_{i1}}{\varepsilon_i^2}, \quad \eta_{i2} = \frac{x_{i2} - \hat{x}_{i2}}{\varepsilon_i}, \quad \eta_{i3} = F_i - \hat{F}_i$$

The observation error equation of state can be written as

$$\varepsilon_i \dot{\eta}_i = \bar{A}_i \eta_i + \varepsilon_i \bar{B}_i \dot{\tilde{F}}_i \tag{21}$$

where

$$\bar{A}_i = \begin{bmatrix} -\alpha_{i1} & 1 & 0 \\ -\alpha_{i2} & 0 & 1 \\ -\alpha_{i3} & 0 & 0 \end{bmatrix}, \quad \bar{B}_i = \begin{bmatrix} 0 \\ 0 \\ 1 \end{bmatrix}$$

The error in position and velocity for heterogeneous systems within the XY plane is defined as follows

$$\begin{aligned} e_i^{x1} &= \sum_{j \in \Pi} a_{ij} ((x_{1i} - x_{1j}) - (\delta_i - \delta_j)) \\ &+ b_i (x_{1i} - x_{1l} - \delta_i) \end{aligned} \tag{22}$$

$$e_i^{x2} = \sum_{j \in \Pi} a_{ij} (x_{2i} - x_{2j}) + b_i (x_{2i} - x_{2l}) \tag{23}$$

The formation control term is designed as follows

$$u_i^f = \frac{1}{\vartheta_i} [-\hat{F}_i - k_i(e_i^{x_1} + e_i^{x_2})] \tag{24}$$

Furthermore, the distributed formation controller with collision avoidance performance can be defined as follows

$$u_i = u_i^f + u_i^{ca} \tag{25}$$

Remark 1. In the formation controller (25), the distributed formation control term u_i^f is used by tracking the time-varying velocity variable of the leader. The virtual repulsive force term u_i^{ca} is used to achieve the collision avoidance objective among the agents. By designing the action functions (14) and (15) of the APF, they are non-conflicting items.

Using (17) and (24), distributed formation controller (25) can be given as

$$u_i = \frac{1}{\vartheta_i} [-\hat{F}_i - k_i(e_i^{x_1} + e_i^{x_2})] - \frac{\omega_i}{\vartheta_i} \sum_{j \in \Pi^c} \nabla_{(p,v)} \varphi_{ij}(p, v) \tag{26}$$

Take the derivative of (13) and substitute (11) and (12) into it. Define the derivatives of the error variables and write them in vector form as follows

$$\dot{Z} = -[M \otimes I_m]Z + \begin{bmatrix} 0_{nm} \\ F_{xi} \end{bmatrix} + \begin{bmatrix} 0_{nm} \\ U \end{bmatrix} + \begin{bmatrix} 0_{nm} \\ \Delta_{xi} \end{bmatrix} - \begin{bmatrix} 0_{nm} \\ F_l \end{bmatrix} \tag{27}$$

where $\dot{Z} = [\dot{\hat{x}}_{11}^T, \dots, \dot{\hat{x}}_{n1}^T, \dot{\hat{x}}_{12}^T, \dots, \dot{\hat{x}}_{n2}^T]^T$, $U = G_{xi}u_{xi}$, $M = \begin{bmatrix} 0_n & -I_n \\ 0_n & 0_n \end{bmatrix}$, \otimes denotes the Kronecker product.

3.2. Altitude Controller Design for UAV

The error system of altitude is defined as

$$e_{zp} = p_{az} - c_p \tag{28}$$

$$e_{zv} = v_{az} - c_v \tag{29}$$

where the desired position signal is c_p and the desired velocity signal is c_v .

The adaptive laws and control input of formation tracking are constructed as

$$u_{az} = \hat{H}_{az}^{-1} \left(-\sigma e_\zeta - \frac{e_\zeta \hat{\kappa}_{11} \omega_1^T \omega_1}{2\zeta_1^2} - \frac{e_\zeta \hat{\kappa}_{12}}{2\zeta_2^2} + \dot{c}_v - k_\zeta e_{zv} \right) \tag{30}$$

$$\dot{\hat{\kappa}}_{11} = l_{11} \left(-k_{11} \hat{\kappa}_{11} + \frac{e_\zeta^T e_\zeta \omega_1^T \omega_1}{2\zeta_1^2} \right) \tag{31}$$

$$\dot{\hat{\kappa}}_{12} = l_{12} \left(-k_{12} \hat{\kappa}_{12} + \frac{e_\zeta^T e_\zeta}{2\zeta_2^2} \right) \tag{32}$$

$$\dot{H}_{az} = \text{Proj}_{[\underline{H}_{az}, \bar{H}_{az}]} \{ \mathcal{F} \} = \begin{cases} 0, & \text{if } \hat{H}_{az} = \bar{H}_{az} \\ & \text{and } \mathcal{F} \geq 0 \\ \text{or } \hat{H}_{az} = \underline{H}_{az} \\ & \text{and } \mathcal{F} \leq 0 \\ \mathcal{F}, & \text{otherwise} \end{cases} \quad (33)$$

where $\mathcal{F} = l_{13}(-k_{13}\hat{H}_{az} + e_{\zeta}u_{az})$, \underline{H}_{az} , and \bar{H}_{az} are the parameter H_{az} 's lower bound and upper bound of, respectively, where $\sigma, k_{11}, k_{12}, k_{13}, k_{\zeta}, l_{11}, l_{12}, l_{13}, \varsigma_1, \varsigma_2$ denote positive parameters.

3.3. Stability Analysis

- **Part A. Proof of the stability of the extended state observer**

Consider the following Lyapunov function

$$V_0 = \sum_{i=1}^{N+1} V_{0i} \quad (34)$$

where V_{0i} is given as

$$V_{0i} = \varepsilon_i \eta_i^T P_i \eta_i \quad (35)$$

$$\begin{aligned} \dot{V}_{0i} &= \varepsilon_i \dot{\eta}_i^T P_i \eta_i + \varepsilon_i \eta_i^T P_i \dot{\eta}_i \\ &= (\bar{A}_i \eta_i + \varepsilon_i \bar{B}_i \dot{F}_i)^T P_i \eta_i + \eta_i^T P_i (\bar{A}_i \eta_i + \varepsilon_i \bar{B}_i \dot{F}_{ni}) \\ &= \eta_i^T \bar{A}_i^T P_i \eta_i + \varepsilon_i (\bar{B}_i \dot{F}_{ni})^T P_i \eta_i \\ &\quad + \eta_i^T P_i \bar{A}_i \eta_i + \varepsilon \eta_i^T P_i \bar{B}_i \dot{F}_{ni} \\ &= \eta_i^T (\bar{A}_i^T P_i + P_i \bar{A}_i) \eta_i + 2\varepsilon_i \eta_i^T P_i \bar{B}_i \dot{F}_{ni} \\ &\leq -\eta_i^T Q_i \eta_i + 2\varepsilon_i \|P_i \bar{B}_i\| \cdot \|\eta_i\| \cdot |\dot{F}_i| \end{aligned} \quad (36)$$

and

$$\dot{V}_{0i} \leq -\lambda_{\min}(Q_i) \|\eta_i\|^2 + 2\varepsilon_i |\dot{F}_i| \|P_i \bar{B}_i\| \|\eta_i\| \quad (37)$$

Therefore, the convergence condition of the observer satisfies

$$\|\eta_i\| \leq \frac{2\varepsilon_i |\dot{F}_i| \|P_i \bar{B}_i\|}{\lambda_{\min}(Q_i)} \quad (38)$$

where Q_i denotes any given symmetric positive definite matrix, $\lambda_{\min}(Q_i)$ is the minimum eigenvalue of Q_i , and there is a three-by-three symmetric positive definite matrix P_i that satisfies the following equation

$$\bar{A}_i^T P_i + P_i \bar{A}_i + Q_i = 0 \quad (39)$$

Remark 2. Based on Assumptions 2 and 3, both the velocity and acceleration of the agent, as well as the external disturbances, are bounded. From $F_i = F_{xi} + \Delta_{xi}$, it is evident that F_i encompasses the agent's velocity and acceleration, as well as external disturbances. So, $|\dot{F}_i|$ is bounded.

- **Part B. Proof of the stability of the system**

Define the Lyapunov quadratic scalar function as follows

$$V_1 = \frac{1}{2} \bar{Z}^T (P_g \otimes I_m) \bar{Z} \tag{40}$$

where $P = \begin{bmatrix} 2\tilde{L}_g & \tilde{L}_g \\ \tilde{L}_g & \tilde{L}_g \end{bmatrix}$, $\tilde{L}_g = L_g + B_g$.

According to Theorem 4, the Lyapunov quadratic scalar function V_1 is a positive definite function.

Substitute (27) into \dot{V}_1 and expand the partial matrix as follows

$$\begin{aligned} \dot{V}_1 &= \bar{Z}^T (P_g \otimes I_m) \dot{\bar{Z}} \\ &= -\frac{1}{2} \bar{Z}^T \left((M^T P_g + P_g M) \otimes I_m \right) \bar{Z} + \bar{Z}^T (P_g \otimes I_m) \begin{bmatrix} 0_{nm} \\ F_{xi} + U + \Delta_{xi} - F_l \end{bmatrix} \\ &= -\bar{Z}^T \left(\begin{bmatrix} 0_n & -\tilde{L}_g \\ -\tilde{L}_g & -\tilde{L}_g \end{bmatrix} \otimes I_m \right) \bar{Z} + \sum_{i=1}^n (e_i^{x1} + e_i^{x2})^T (F_{xi} + G_{xi} u_{xi} + \Delta_{xi} - F_l) \end{aligned} \tag{41}$$

Substituting the distributed formation controller (24) into (41), we can obtain

$$\begin{aligned} \dot{V}_1 &= -\bar{Z}^T \left(\begin{bmatrix} 0_n & -\tilde{L}_g \\ -\tilde{L}_g & -\tilde{L}_g \end{bmatrix} \otimes I_m \right) \bar{Z} \\ &\quad + \sum_{i=1}^n (e_i^{x1} + e_i^{x2})^T F_{xi} - \sum_{i=1}^n (e_i^{x1} + e_i^{x2})^T F_l + \sum_{i=1}^n (e_i^{x1} + e_i^{x2})^T \\ &\quad \times \left(-\hat{F}_i - k_i (e_i^{x1} + e_i^{x2}) - \omega_i \sum_{j \in \Pi^c} \nabla_{(p,v)} \varphi_{ij}(p, v) \right) \\ &= -\bar{Z}^T \left(\begin{bmatrix} 0_n & -\tilde{L}_g \\ -\tilde{L}_g & -\tilde{L}_g \end{bmatrix} \otimes I_m \right) \bar{Z} - \sum_{i=1}^n (e_i^{x1} + e_i^{x2})^T F_l \\ &\quad - \sum_{i=1}^n k_i \| (e_i^{x1} + e_i^{x2}) \|^2 - \sum_{i=1}^n (e_i^{x1} + e_i^{x2})^T \times \omega_i \sum_{j \in \Pi^c} \nabla_{(p,v)} \varphi_{ij}(p, v) \end{aligned} \tag{42}$$

In the case of an undirected graph, the Laplacian matrix exhibits symmetry, and the virtual repulsive force term u_i^{ca} becomes negligible once collision avoidance is achieved through the repulsive potential function $\varphi_{ij}(p, v)$.

Therefore, the aforementioned term $V' = -\sum_{i=1}^n (e_i^{x1} + e_i^{x2})^T \omega_i \sum_{j \in \Pi^c} \nabla_{(p,v)} \varphi_{ij}(p, v) = 0$, based on Assumption 1 and Young's inequality as follows

$$-(e_i^{x1} + e_i^{x2})^T F_l \leq \zeta_i \|e_i^{x1} + e_i^{x2}\|^2 + \frac{\alpha_l^2}{4\zeta_i}$$

where ζ_i is a positive constant.

And then the results (42) can be derived as follows

$$\begin{aligned} \dot{V}_1 &\leq -\bar{Z}^T \left(\begin{bmatrix} 0_n & -\tilde{L}_g \\ -\tilde{L}_g & -\tilde{L}_g \end{bmatrix} \otimes I_m \right) \bar{Z} + \sum_{i=1}^n \zeta_i \|e_i^{x1} + e_i^{x2}\|^2 + \sum_{i=1}^n \frac{\alpha_l}{4\zeta_i} - \sum_{i=1}^n k_i \| (e_i^{x1} + e_i^{x2}) \|^2 \\ &= -\bar{Z}^T \left(\begin{bmatrix} 0_n & -\tilde{L}_g \\ -\tilde{L}_g & -\tilde{L}_g \end{bmatrix} \otimes I_m \right) \bar{Z} + \sum_{i=1}^n (\zeta_i - k_i) \|e_i^{x1} + e_i^{x2}\|^2 + \sum_{i=1}^n \frac{\alpha_l^2}{4\zeta_i} \end{aligned} \tag{43}$$

Let ρ_i satisfy the limit of $\rho_i \leq k_i - \zeta_i$ and $\rho_i > 0$, the inequality is transformed into

$$\begin{aligned} \dot{V}_1 &\leq -\bar{Z}^T \left(\begin{bmatrix} 0_n & -\tilde{L}_g \\ -\tilde{L}_g & -\tilde{L}_g \end{bmatrix} \otimes I_m \right) \bar{Z} - \sum_{i=1}^n \rho_i \|e_i^{x_1} + e_i^{x_2}\|^2 + \sum_{i=1}^n \frac{\alpha_i^2}{4\zeta_i} \\ &= -\bar{Z}^T \left(\left(\rho_i \begin{bmatrix} \tilde{L}_g^2 & \tilde{L}_g^2 \\ \tilde{L}_g^2 & \tilde{L}_g^2 \end{bmatrix} - \begin{bmatrix} 0_n & \tilde{L}_g \\ \tilde{L}_g & \tilde{L}_g \end{bmatrix} \right) \otimes I_m \right) \bar{Z} + \sum_{i=1}^n \frac{\alpha_i^2}{4\zeta_i} \\ &= -\bar{Z}^T \left(\begin{bmatrix} \rho_i \tilde{L}_g^2 & \rho_i \tilde{L}_g^2 - \tilde{L}_g \\ \rho_i \tilde{L}_g^2 - \tilde{L}_g & \rho_i \tilde{L}_g^2 \end{bmatrix} \otimes I_m \right) \bar{Z} + \sum_{i=1}^n \frac{\alpha_i^2}{4\zeta_i} \end{aligned} \tag{44}$$

According to the Lemma of linear matrix inequality in [41], $\rho_i \tilde{L}_g^2 - (\rho_i \tilde{L}_g^2 - \tilde{L}_g) = \tilde{L}_g^2 > 0$, $\rho_i \tilde{L}_g^2 - \tilde{L}_g > 0$, so the matrix $\begin{bmatrix} \rho_i \tilde{L}_g^2 & \rho_i \tilde{L}_g^2 - \tilde{L}_g \\ \rho_i \tilde{L}_g^2 - \tilde{L}_g & \rho_i \tilde{L}_g^2 \end{bmatrix} > 0$. Therefore, the inequality (44) can be rewritten as follows

$$\begin{aligned} \dot{V}_1 &\leq -\bar{Z}^T \left(\left(\rho_i \begin{bmatrix} \tilde{L}_g^2 & \tilde{L}_g^2 \\ \tilde{L}_g^2 & \tilde{L}_g^2 \end{bmatrix} - \begin{bmatrix} 0_n & \tilde{L}_g \\ \tilde{L}_g & \tilde{L}_g \end{bmatrix} \right) \otimes I_m \right) \bar{Z} + \sum_{i=1}^n \frac{\alpha_i^2}{4\zeta_i} \\ &= -\bar{Z}^T ((\rho_i \Theta - \Xi) \otimes I_m) \bar{Z} + \Delta \end{aligned} \tag{45}$$

where

$$\Theta = \begin{bmatrix} \tilde{L}_g^2 & \tilde{L}_g^2 \\ \tilde{L}_g^2 & \tilde{L}_g^2 \end{bmatrix}, \Xi = \begin{bmatrix} 0_n & \tilde{L}_g \\ \tilde{L}_g & \tilde{L}_g \end{bmatrix}, \Delta = \sum_{i=1}^n \frac{\alpha_i^2}{4\zeta_i}.$$

Set $\rho_i > \frac{1}{\lambda_{\min}^{\Theta}} (\lambda_{\max}^{\Xi} + \frac{\mathfrak{S}}{2} \lambda_{\max}^P)$, where $\lambda_{\min}^{\Theta}, \lambda_{\max}^{\Xi}, \lambda_{\max}^P$ denote the smallest eigenvalue of the matrix Θ , the largest eigenvalue of the matrix Ξ , and the largest eigenvalue of the matrix P , respectively, and $\mathfrak{S} = \min\{\sigma_1 Y_1, \dots, \sigma_n Y_n\}$.

Then, we can obtain

$$\begin{aligned} \dot{V}_1 &\leq -\mathfrak{S} \bar{Z}^T (P \otimes I_m) \bar{Z} + \Delta \\ &= -\mathfrak{S} V_1 + \Delta \end{aligned} \tag{46}$$

In accordance with Theorem 1, the subsequent inequality can be presented in the following manner

$$V_1(t) \leq V_1(0)e^{-\mathfrak{S}t} + \frac{\Delta}{\mathfrak{S}}(1 - e^{-\mathfrak{S}t}) \tag{47}$$

Consequently, by choosing suitable parameters as indicated in [44], one can achieve the performance of adaptive leader-following formation.

• **Part C. Proof of collision avoidance**

The collision avoidance performance is analyzed only for the i -th ($i \in \Pi$) USV and its collision avoidance neighbor the j -th ($j \in \Pi^c$) USV, and the others can be analyzed by the same way in [42].

Define the energy function holds quadratic form as follows

$$S(t) = \frac{1}{2} v_i^T(t) v_i(t) + \frac{1}{2} d_{ik}^T(t) d_{ik}(t) \tag{48}$$

Taking the time derivative of (48), we can get

$$\dot{S}(t) = \omega_i v_i^T(t) \nabla_{(p,v)} \varphi_{ij}(p, v) + d_{ik}^T(t) (v_i(t) - v_k(t)) - v_i^T(t) \hat{E}_i - k_i v_i^T(t) (e_i^{x_1}(t) + e_i^{x_2}(t)) \tag{49}$$

where $d_{ik}(t)$ is the relative position variable.

Because of the designing of the repulsive potential function $\varphi_{ij}(p, v)$, $\varphi_i(d_{ik}(t))$ will approach infinity by designing the parameter $\bar{\omega}_i > 0$ if the i -th USV is closing to the j -th USV. Therefore, if the i -th USV and the j -th USV are close to each other, and design the appropriate parameter, the inequality can be met in the following manner:

$$\begin{aligned} v_i^T(t) \nabla_{(p,v)} \varphi_{ij}(p, v) &> \frac{1}{2} d_{ik}^T(t) d_{ik}(t) + \frac{1}{2} v_i^T(t) v_i(t) \\ &- \frac{1}{\omega_i} d_{ik}^T(t) (v_i(t) - v_k(t)) + \frac{1}{\omega_i} v_i^T(t) \hat{F}_i \\ &+ \frac{k_i}{\omega_i} v_i^T(t) (e_i^{x_1}(t) + e_i^{x_2}(t)) \end{aligned} \tag{50}$$

Substituting the aforementioned inequality (50) into (49), the subsequent inequality can be derived

$$\dot{S}(t) > \omega_i S(t)$$

Based on the principles outlined in Theorem 2, the subsequent inequality can be derived

$$d_{ik}^T(t) d_{ik}(t) > 2e^{\omega_i(t-t_0)} S(t) - v_i^T(t) v_i(t)$$

Since the previously indicated term $v_i^T(t) v_i(t)$ is continuous and bounded at this dwell time. By designing the gain parameter $\omega_i > 0$ large enough, we get can the inequality $2e^{\omega_i(t-t_0)} S(t) - v_i^T(t) v_i(t) > (2r_1)^2$ and the result can be obtained as $\|d_{ik}(t)\| > 2r_1$. As a result, the collision avoidance performance can be guaranteed by the proposed formation control with collision avoidance strategy.

• **Part D. Proof of the decentralized formation controller**

If the feasibility condition $c_v - \dot{c}_p = 0$ is satisfied, it then allows the time derivative of Equations (28) and (29) to be expressed as follows

$$\dot{e}_{zp} = e_{zv} \tag{51}$$

$$\dot{e}_{zv} = F_{az} + G_{az} u_{az} + \Delta_{az} - \dot{c}_v. \tag{52}$$

where e_{zv} may be regarded as the virtual control input in the system (51). The stability of the system (51) can be assured by constructing the virtual control input $\zeta = -k_\zeta e_{zp}$.

A positive Lyapunov function is considered as

$$V_{zp} = \frac{1}{2} e_{zp}^T e_{zp} \tag{53}$$

A new error is defined as

$$e_\zeta = e_{zv} - \zeta \tag{54}$$

By computing the time derivative of Equation (53) and incorporating the control input from Equation (30) into this calculation, one can obtain

$$\dot{e}_\zeta = -\sigma e_\zeta + F_{az} + \Delta_{az} + \tilde{H}_{az} u_{az} - \frac{e_\zeta \hat{\kappa}_{11} \omega_1^T \omega_1}{2\zeta_1^2} - \frac{e_\zeta \hat{\kappa}_{12}}{2\zeta_2^2}. \tag{55}$$

V_z is given as

$$V_z = \frac{1}{2} e_{zp}^T e_{zp} + \frac{1}{2} e_\zeta^T e_\zeta + \frac{\hat{\kappa}_{11}^2}{2l_{11}} + \frac{\hat{\kappa}_{12}^2}{2l_{12}} + \frac{\text{Tr}(\tilde{H}_{az}^T \tilde{H}_{az})}{2l_{13}} \tag{56}$$

with $\tilde{\kappa}_{11} = \kappa_{11} - \hat{\kappa}_{11}$, $\tilde{\kappa}_{12} = \kappa_{12} - \hat{\kappa}_{12}$ and $\tilde{H}_{az} = H_{az} - \hat{H}_{az}$.

$$\begin{aligned} \dot{V}_z \leq & -k_\zeta e_{zp}^T e_{zp} - \sigma e_\zeta^T e_\zeta + e_\zeta^T F_{az} + e_\zeta^T \Delta_{az} \\ & + e_\zeta^T \tilde{H}_{az} u_{az} - \frac{e_\zeta^T e_\zeta \hat{\kappa}_{11} \omega_1^T \omega_1}{2\zeta_1^2} - \frac{e_\zeta^T e_\zeta \hat{\kappa}_{12}}{2\zeta_2^2} + \frac{\tilde{\kappa}_{11} \dot{\hat{\kappa}}_{11}}{l_{11}} + \frac{\tilde{\kappa}_{12} \dot{\hat{\kappa}}_{12}}{l_{12}} + \frac{\text{Tr}(\tilde{H}_{az}^T \dot{\hat{H}}_{az})}{l_{13}} \end{aligned} \quad (57)$$

Given that F_{az} is an undefined function, as per the universal approximation theorem cited in [45], for any arbitrarily small constant ϵ_1 , there exists a fuzzy logic system $\theta_1^{*T} \omega_1$ that can be represented as $F_{az} = \theta_1^{*T} \omega_1 + \epsilon_1$. In this context, θ_1^{*T} represents the optimal weight, ω_1 is the fuzzy basis vector, ϵ_1 denotes the fuzzy system’s approximation error, and it is established that $|\epsilon_1| \leq \bar{\epsilon}_1$.

Regarding Young’s inequality, it can be deduced that

$$e_\zeta^T \theta_1^{*T} \omega_1 \leq \frac{e_\zeta^T e_\zeta \kappa_{11} \omega_1^T \omega_1}{2\zeta_1^2} + \frac{\zeta_1^2}{2} \quad (58)$$

$$e_\zeta^T (\epsilon_1 + \Delta_{az}) \leq \frac{e_\zeta^T e_\zeta \kappa_{12}}{2\zeta_2^2} + \frac{\zeta_2^2}{2} \quad (59)$$

where $\kappa_{11} = \theta_1^{*T} \theta_1^*$ and $\kappa_{12} = (\bar{\epsilon}_1 + \bar{\Delta}_{az})^T (\bar{\epsilon}_1 + \bar{\Delta}_{az})$.

Substituting (58) and (59) into (57), we can obtain

$$\begin{aligned} \dot{V}_z \leq & -k_\zeta e_{zp}^T e_{zp} - \sigma e_\zeta^T e_\zeta + \frac{e_\zeta^T e_\zeta \kappa_{11} \omega_1^T \omega_1}{2\zeta_1^2} + \frac{e_\zeta^T e_\zeta \kappa_{12}}{2\zeta_2^2} \\ & - \frac{e_\zeta^T e_\zeta \hat{\kappa}_{11} \omega_1^T \omega_1}{2\zeta_1^2} - \frac{e_\zeta^T e_\zeta \hat{\kappa}_{12}}{2\zeta_2^2} - \tilde{\kappa}_{12} \left(-k_{12} \hat{\kappa}_{12} + \frac{e_\zeta^T e_\zeta}{2\zeta_2^2} \right) \\ & - \tilde{\kappa}_{11} \left(-k_{11} \hat{\kappa}_{11} + \frac{e_\zeta^T e_\zeta \omega_1^T \omega_1}{2\zeta_1^2} \right) + e_\zeta^T \tilde{H}_{az} u_{az} \\ & - \text{Tr}(\tilde{H}_{az}^T (-k_{13} \hat{H}_{az} + e_\zeta u_{az})) + \frac{\zeta_1^2}{2} + \frac{\zeta_2^2}{2} \\ \leq & -k_\zeta e_{zp}^T e_{zp} - \sigma e_\zeta^T e_\zeta - \frac{k_{11}}{2} \tilde{\kappa}_{11}^2 - \frac{k_{12}}{2} \tilde{\kappa}_{12}^2 - \frac{k_{13}}{2} \|\tilde{H}_{az}\|_F^2 \\ & + \frac{k_{11}}{2} \kappa_{11}^2 + \frac{k_{12}}{2} \kappa_{12}^2 + \frac{k_{13}}{2} \|H_{az}\|_F^2 + \frac{\zeta_1^2}{2} + \frac{\zeta_2^2}{2} \\ \leq & -\vartheta_z V_z + v_z \end{aligned} \quad (60)$$

where $\vartheta_z = \min\{2k_\zeta, 2\sigma, l_{11}k_{11}, l_{12}k_{12}, l_{13}k_{13}\} > 0$, $v_z = \frac{k_{11}}{2} \kappa_{11}^2 + \frac{k_{12}}{2} \kappa_{12}^2 + \frac{k_{13}}{2} \|H_{az}\|_F^2 + \frac{\zeta_1^2}{2} + \frac{\zeta_2^2}{2}$.

Based on Equation (60), \dot{V}_z is derived as follows

$$\dot{V}_z \leq -\vartheta_z V_z + v_z \quad (61)$$

According to the boundedness theorem, the closed-loop system solution is uniformly eventually bounded. Using e_{zp} and e_ζ , it is possible to deduce that the UAV’s velocity error and altitude tracking error are uniformly eventually bounded.

4. Simulation Result

In this section, a simulation analysis for the heterogeneous systems with collision avoidance performance under parameter uncertainty and external disturbance is provided to illustrate the effect of the proposed approach. One UAV and four USVs make up the

heterogeneous system. The simulation experiments described in this section were executed on the MATLAB R2020a simulation platform.

The communication topology is defined in Figure 3, where agent l represents the virtual leader, agent 0 represents the UAV, and agents 1–4 represent the four USVs. If $B_g = \text{diag}\{0, 0, 0, 0, 1\}$ is the adjacency weight matrix between agents and the virtual leader, then the adjacency matrix A_g and the Laplacian matrix L_g are as follows:

$$A_g = \begin{bmatrix} 0 & 1 & 1 & 0 & 1 \\ 1 & 0 & 1 & 1 & 0 \\ 1 & 1 & 0 & 0 & 0 \\ 0 & 1 & 0 & 0 & 0 \\ 1 & 0 & 0 & 0 & 0 \end{bmatrix} \quad L_g = \begin{bmatrix} 3 & -1 & -1 & 0 & -1 \\ -1 & 3 & -1 & -1 & 0 \\ -1 & -1 & 2 & 0 & 0 \\ 0 & -1 & 0 & 1 & 0 \\ -1 & 0 & 0 & 0 & 1 \end{bmatrix}$$

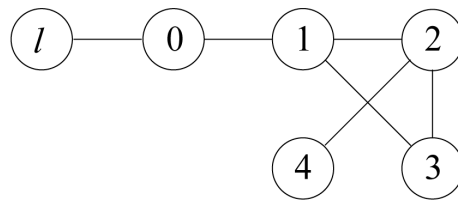


Figure 3. Communication topology graph.

The system parameters of a UAV and USVs are given in Tables 1 and 2, respectively. APF design parameters $r_{in} = 0.5, r_{out} = 2, \bar{\omega}_i = 0.3, \omega_i = 1$, where $i = 1, \dots, 4$. The external disturbances are given as $\Delta_{axy} = [0.2 \cos(0.5t), 0.8 \cos(t)]^T, \Delta_{az} = 0.3 \cos(0.2t), w_{biyy} = [1.1 \cos(0.5t), -0.2 \sin(2t)]^T$. The total duration of the simulation runs $T_z = 80$ s and the sampling time $T_s = 0.6$ s.

Table 1. The model parameters of UAV.

Parameter	Value	Unit
m_a	2	kg
g_a	9.8	$m \cdot s^{-2}$
J_{ax}, J_{ay}, J_{az}	1.5	$N \cdot s^2 \cdot \text{rad}^{-1}$
d_{ax}, d_{ay}, d_{az}	0.012	$N \cdot s^2 \cdot \text{rad}^{-1}$

Table 2. The model parameters of USV.

Parameter	Value	Unit
$m_{\mu bi}$	25.8	kg
$m_{v bi}$	33.8	kg
$m_{r bi}$	2.76	kg
$d_{\mu bi}$	0.725	$kg \cdot s^{-1}$
$d_{v bi}$	0.89	$kg \cdot s^{-1}$
$d_{r bi}$	-1.9	$kg \cdot m^{-2} \cdot s^{-1}$
$d_{\mu bi1}$	-1.33	$kg \cdot s^{-1}$
$d_{v bi1}$	-36.47	$kg \cdot s^{-1}$
$d_{r bi1}$	-0.75	$kg \cdot m^{-2} \cdot s^{-1}$

The initial position state vector of the UAV and USVs are defined as $x_0(0) = [6, 2, 10]^T, x_1(0) = [8, 0, 0]^T, x_2(0) = [4, 0, 0]^T, x_3(0) = [4, 4, 0]^T, x_4(0) = [8, 4, 0]^T, \delta_0 = [0, 0]^T, \delta_1 = [0, 3\aleph]^T, \delta_2 = [-\sqrt{3}\aleph, 0]^T, \delta_3 = [\sqrt{3}\aleph, 0]^T, \delta_4 = [0, \aleph]^T, \aleph = \frac{3}{2}$.

The simulation results by using the proposed control method for heterogeneous systems with collision avoidance strategy are shown in Figures 4–11. The trajectories of the four USVs and the UAV in the 3D environment are depicted in Figure 4. The black line represents the UAV’s trajectory, while the other color lines represent the trajectories of the

four USVs. From the given starting point, the USVs maintain a safe distance and establish a designated configuration between each other. Figure 5 shows the trajectories of heterogeneous systems without collision avoidance. At the sampling time $T_s = 0.6$ s, Figure 5 shows that three USVs have been collided. Simulation trajectory plots demonstrate the importance of collision avoidance for heterogeneous systems.

Figure 6 and 7 represent the position tracking errors and velocity errors in x-label and y-label, respectively. Under the influence of external disturbances and parameter uncertainties, the formation trajectory tracking errors are capable of converging to a minimal residual set. Figures 8 and 9 depict the surge force and yaw torque. The outcomes of the simulations indicate that the USVs are able to continue tracking the virtual leader even after activating the improved APF for collision avoidance.

Figures 10 and 11 further display the distances between USVs without and with considering the collision avoidance. Figure 10 shows that the USVs have collided, because of the distance $\|d_{ij}\|_{\min} < 2r_1 = 1$. Figure 11 shows that the distances of USVs can always maintain $\|d_{ij}\|_{\min} > 2r_1 = 1$ at any time. The simulation diagrams further confirm that the proposed formation control with collision avoidance strategy has an excellent performance. The performance of ESO in estimating F_i is depicted in Figure 12, which clearly demonstrates the effectiveness of the proposed solution for the accurate compensation of uncertainties and external disturbances within heterogeneous systems.

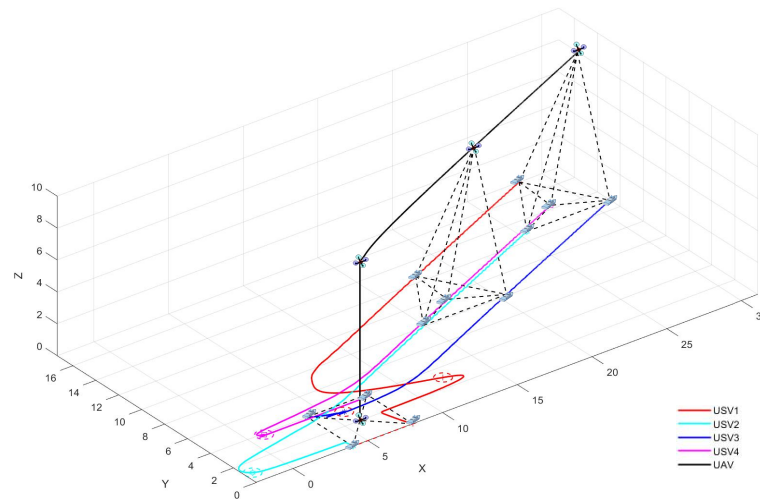


Figure 4. Formation evolution of heterogeneous systems with collision avoidance.

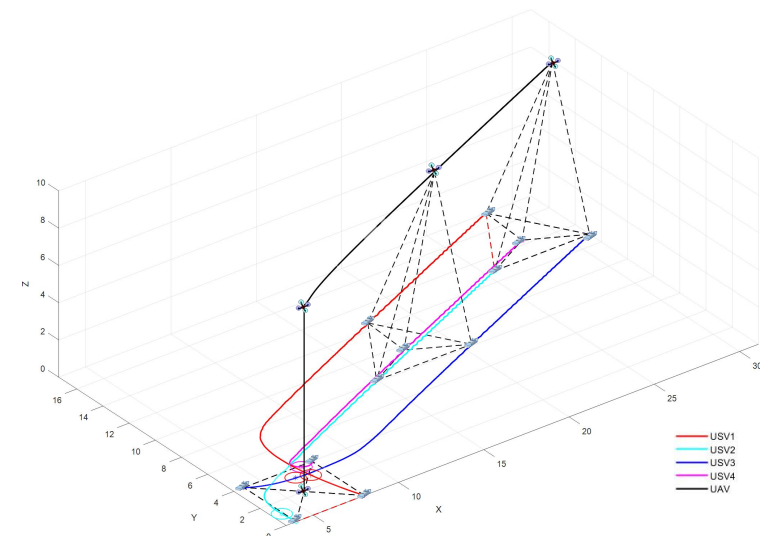


Figure 5. Formation evolution of heterogeneous systems without collision avoidance.

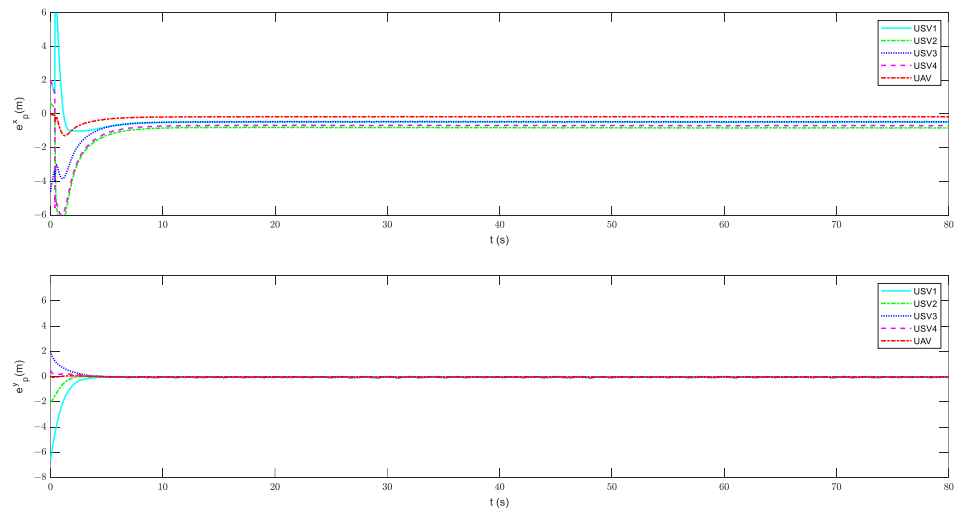


Figure 6. Position tracking errors of the UAV and USVs with collision avoidance.

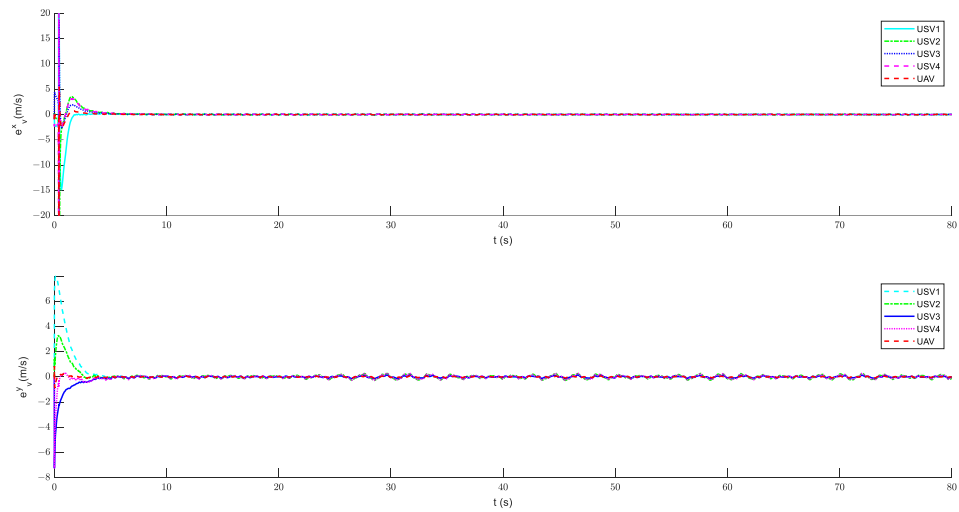


Figure 7. Velocity errors of the UAV and USVs with collision avoidance.

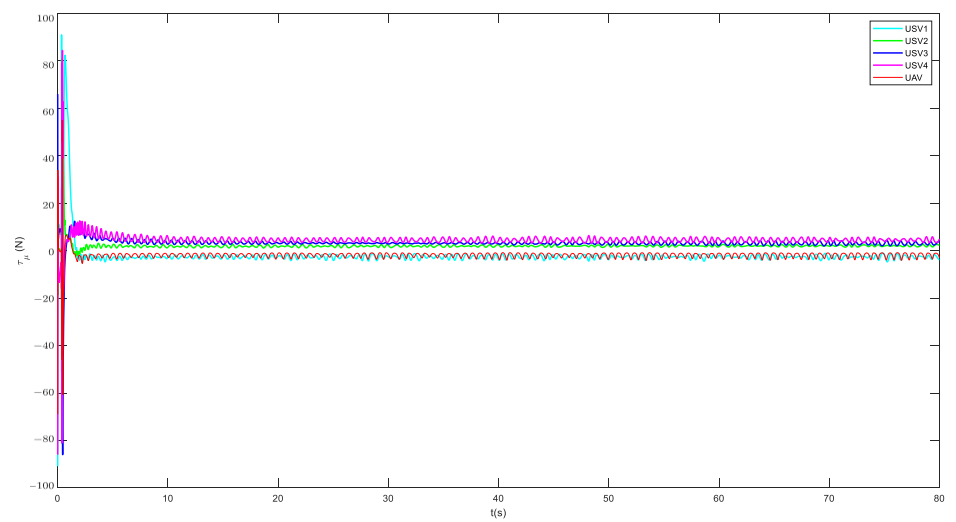


Figure 8. The surge force of heterogeneous system.

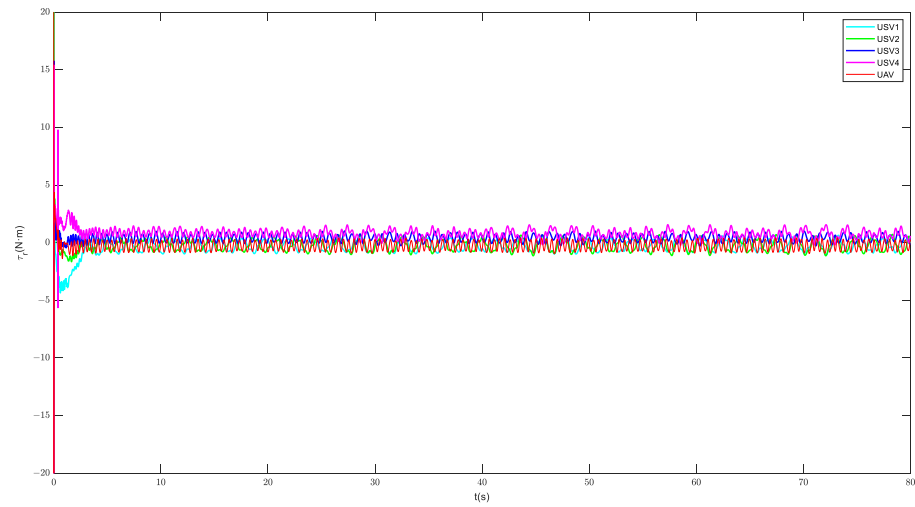


Figure 9. The yaw torque of heterogeneous system.

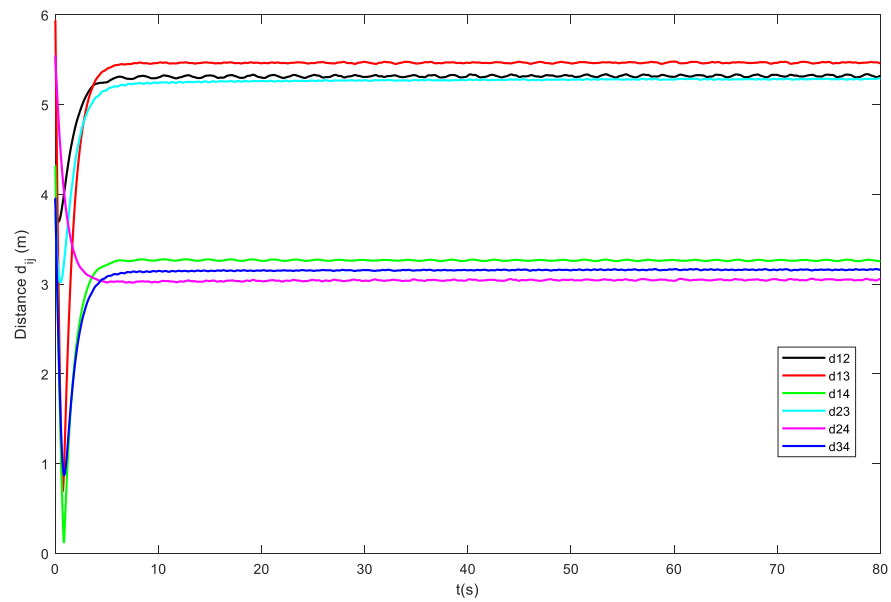


Figure 10. The distance between the USVs without collision avoidance.

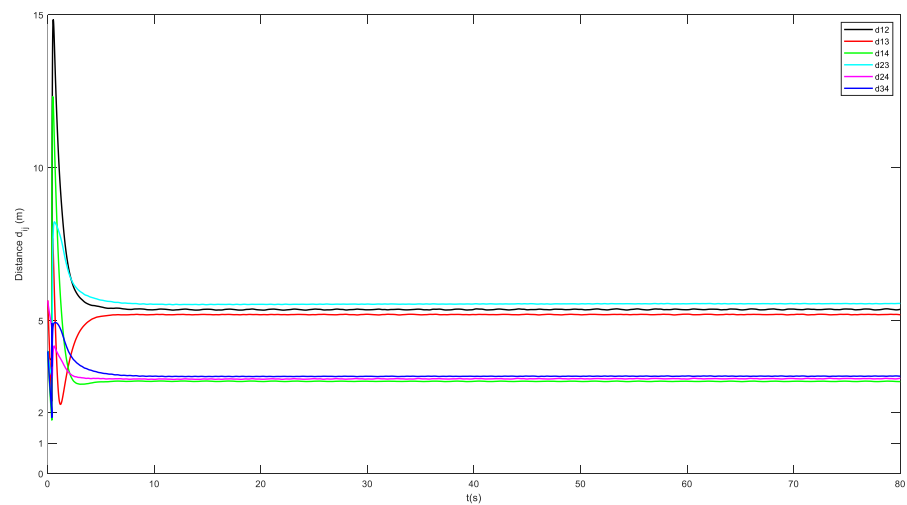


Figure 11. The distance between the USVs with collision avoidance.

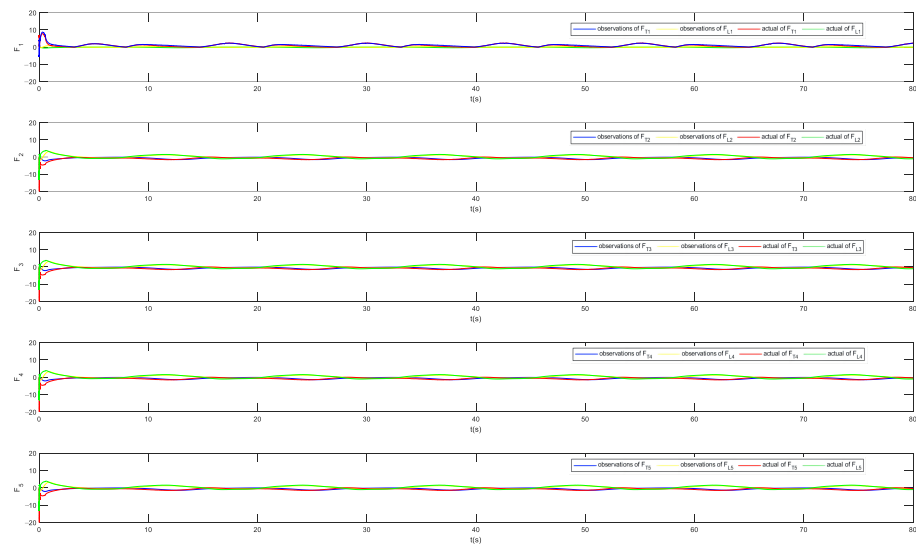


Figure 12. The estimated performance of ESO.

5. Conclusions

In this paper, the cooperative formation trajectory tracking problem for heterogeneous systems with collision avoidance performance under parameter uncertainty and external disturbance is investigated. Under the unified dynamic model of a UAV and USVs in the XY plane, a formation control protocol based on ESO is proposed. The collision avoidance control approach for USV formation is then constructed using APF theory. Furthermore, the APF approach is improved by rebuilding the repulsive potential field to bring the unmanned ship's collision avoidance behavior more in compliance with COLREGs. According to the Lyapunov stability theory, the time-varying formation errors and tracking errors are uniformly ultimately limited. Simulation results verify the effectiveness of the proposed scheme.

This paper focuses solely on heterogeneous formation and collision avoidance between a single UAV and multiple USVs. Going forward, cooperative collision avoidance involving multiple UAVs and USVs within intricate environments deserves further study. In discussions of formation control issues for multi-agent or multi-vehicle systems, it is common to assume that the controlled entities operate within an ideal network communication environment. However, in practical scenarios, such as with USVs, the communication environment is often fraught with issues like noise, time delays, and packet loss. Consequently, the problem of cooperative collision avoidance control for swarm systems under adverse communication conditions also merits thorough investigation.

Author Contributions: Conceptualization, Y.H. and J.N.; methodology, Y.H. and J.N.; software, Y.H.; validation, Y.H.; writing—original draft preparation, Y.H.; writing—review and editing, Y.H., W.L., J.N. and Z.L.; supervision, W.L. and J.N.; project administration, W.L. and Z.L.; funding acquisition, W.L. and J.N. All authors have read and agreed to the published version of the manuscript.

Funding: This work was supported in part by the National Natural Science Foundation of China under Grants 52271304, and 61976033, and in part by the Fundamental Research Funds for the Central Universities under Grant 3132023151.

Institutional Review Board Statement: Not applicable.

Informed Consent Statement: Not applicable.

Data Availability Statement: Data are contained within the article.

Conflicts of Interest: The authors declare no conflict of interest.

Abbreviations

The following abbreviations are used in this manuscript:

UAV	Unmanned Aerial Vehicle
UGV	Unmanned Ground Vehicle
USV	Unmanned Surface Vehicle
AUV	Autonomous Underwater Vehicle
ESO	Extended State Observer
APF	Artificial Potential Field
COLREG	International Regulations for Preventing Collisions at Sea
RBF	Radial Basis Function

References

1. Yan, X.; Jiang, D.; Miao, R.; Li, Y. Formation control and obstacle avoidance algorithm of a multi-USV system based on virtual structure and artificial potential field. *J. Mar. Sci. Eng.* **2021**, *9*, 161. [\[CrossRef\]](#)
2. Shan, Q.; Wang, X.; Li, T.; Chen, C.P. Finite-time control for USV path tracking under input saturation with random disturbances. *Appl. Ocean Res.* **2023**, *138*, 103628. [\[CrossRef\]](#)
3. Guerrero-Ibañez, J.; Contreras-Castillo, J.; Zeadally, S. Deep learning support for intelligent transportation systems. *Trans. Emerg. Telecommun. Technol.* **2021**, *32*, e4169. [\[CrossRef\]](#)
4. Li, X.; Tan, J.; Liu, A.; Vijayakumar, P.; Kumar, N.; Alazab, M. A Novel UAV-Enabled Data Collection Scheme for Intelligent Transportation System Through UAV Speed Control. *IEEE Trans. Intell. Transp. Syst.* **2021**, *22*, 2100–2110. [\[CrossRef\]](#)
5. Menouar, H.; Guvenc, I.; Akkaya, K.; Uluagac, A.S.; Kadri, A.; Tuncer, A. UAV-Enabled Intelligent Transportation Systems for the Smart City: Applications and Challenges. *IEEE Commun. Mag.* **2017**, *55*, 22–28. [\[CrossRef\]](#)
6. Sun, Y.; Zhang, D.; Wang, Y.; Zong, Z.; Wu, Z. Model Experimental Study on a T-Foil Control Method with Anti-Vertical Motion Optimization of the Mono Hull. *J. Mar. Sci. Eng.* **2023**, *11*, 1551. [\[CrossRef\]](#)
7. Ke, C.; Chen, H. Cooperative path planning for air–sea heterogeneous unmanned vehicles using search-and-tracking mission. *Ocean Eng.* **2022**, *262*, 112020. [\[CrossRef\]](#)
8. Ren, Y.; Zhang, L.; Ying, Y.; Li, S.; Tang, Y. Model-Parameter-Free Prescribed Time Trajectory Tracking Control for Under-Actuated Unmanned Surface Vehicles with Saturation Constraints and External Disturbances. *J. Mar. Sci. Eng.* **2023**, *11*, 1717. [\[CrossRef\]](#)
9. Peng, Z.; Wang, J.; Wang, D. Distributed maneuvering of autonomous surface vehicles based on neurodynamic optimization and fuzzy approximation. *IEEE Trans. Control Syst. Technol.* **2017**, *26*, 1083–1090. [\[CrossRef\]](#)
10. Zhou, Z.; Li, M.; Hao, Y. A Novel Region-Construction Method for Multi-USV Cooperative Target Allocation in Air–Ocean Integrated Environments. *J. Mar. Sci. Eng.* **2023**, *11*, 1369. [\[CrossRef\]](#)
11. Fu, H.; Yao, W.; Cajo, R.; Zhao, S. Trajectory Tracking Predictive Control for Unmanned Surface Vehicles with Improved Nonlinear Disturbance Observer. *J. Mar. Sci. Eng.* **2023**, *11*, 1874. [\[CrossRef\]](#)
12. Gu, N.; Wang, D.; Peng, Z.; Liu, L. Distributed containment maneuvering of uncertain under-actuated unmanned surface vehicles guided by multiple virtual leaders with a formation. *Ocean Eng.* **2019**, *187*, 105996. [\[CrossRef\]](#)
13. Tan, G.; Zhuang, J.; Zou, J.; Wan, L. Multi-type task allocation for multiple heterogeneous unmanned surface vehicles (USVs) based on the self-organizing map. *Appl. Ocean Res.* **2022**, *126*, 103262. [\[CrossRef\]](#)
14. Peng, Z.; Wang, D.; Chen, Z.; Hu, X.; Lan, W. Adaptive dynamic surface control for formations of autonomous surface vehicles with uncertain dynamics. *IEEE Trans. Control Syst. Technol.* **2012**, *21*, 513–520. [\[CrossRef\]](#)
15. Miao, R.; Wang, L.; Pang, S. Coordination of distributed unmanned surface vehicles via model-based reinforcement learning methods. *Appl. Ocean Res.* **2022**, *122*, 103106. [\[CrossRef\]](#)
16. Li, J.; Zhang, G.; Shan, Q.; Zhang, W. A novel cooperative design for USV-UAV systems: 3D mapping guidance and adaptive fuzzy control. *IEEE Trans. Control. Netw. Syst.* **2022**, *10*, 564–574. [\[CrossRef\]](#)
17. Peng, Z.; Wang, J.; Wang, D.; Han, Q.L. An overview of recent advances in coordinated control of multiple autonomous surface vehicles. *IEEE Trans. Ind. Inform.* **2020**, *17*, 732–745. [\[CrossRef\]](#)
18. Liu, H.; Weng, P.; Tian, X.; Mai, Q. Distributed adaptive fixed-time formation control for UAV-USV heterogeneous multi-agent systems. *Ocean Eng.* **2023**, *267*, 113240. [\[CrossRef\]](#)
19. Liu, W.; Ye, H.; Yang, X. Model-Free Adaptive Sliding Mode Control Method for Unmanned Surface Vehicle Course Control. *J. Mar. Sci. Eng.* **2023**, *11*, 1904. [\[CrossRef\]](#)
20. Huang, C.; Zhang, X.; Zhang, G.; Deng, Y. Robust practical fixed-time leader–follower formation control for underactuated autonomous surface vessels using event-triggered mechanism. *Ocean Eng.* **2021**, *233*, 109026. [\[CrossRef\]](#)
21. Li, J.; Zhang, G.; Li, B. Robust adaptive neural cooperative control for the USV-UAV based on the LVS-LVA guidance principle. *J. Mar. Sci. Eng.* **2022**, *10*, 51. [\[CrossRef\]](#)
22. Tan, G.; Zhuang, J.; Zou, J.; Wan, L. Coordination control for multiple unmanned surface vehicles using hybrid behavior-based method. *Ocean Eng.* **2021**, *232*, 109147. [\[CrossRef\]](#)
23. Huang, D.; Li, H.; Li, X. Formation of Generic UAVs-USVs System Under Distributed Model Predictive Control Scheme. *IEEE Trans. Circuits Syst. II Express Briefs* **2020**, *67*, 3123–3127. [\[CrossRef\]](#)

24. Wang, N.; Ahn, C.K. Coordinated Trajectory-Tracking Control of a Marine Aerial-Surface Heterogeneous System. *IEEE/ASME Trans. Mechatronics* **2021**, *26*, 3198–3210. [[CrossRef](#)]
25. Liu, S.; Jiang, B.; Mao, Z.; Ma, Y. Adaptive Fault-Tolerant Formation Control of Heterogeneous Multi-Agent Systems under Directed Communication Topology. *Sensors* **2022**, *22*, 6212. [[CrossRef](#)] [[PubMed](#)]
26. Li, S.; Wang, X.; Wang, S.; Zhang, Y. Distributed Bearing-Only Formation Control for UAV-UWSV Heterogeneous System. *Drones* **2023**, *7*, 124. [[CrossRef](#)]
27. Li, L.; Wu, D.; Huang, Y.; Yuan, Z.M. A path planning strategy unified with a COLREGS collision avoidance function based on deep reinforcement learning and artificial potential field. *Appl. Ocean Res.* **2021**, *113*, 102759. [[CrossRef](#)]
28. Sun, X.; Wang, G.; Fan, Y. Collision avoidance guidance and control scheme for vector propulsion unmanned surface vehicle with disturbance. *Appl. Ocean Res.* **2021**, *115*, 102799. [[CrossRef](#)]
29. Ghommam, J.; Saad, M.; Mnif, F.; Zhu, Q.M. Guaranteed Performance Design for Formation Tracking and Collision Avoidance of Multiple USVs With Disturbances and Unmodeled Dynamics. *IEEE Syst. J.* **2021**, *15*, 4346–4357. [[CrossRef](#)]
30. Dai, S.L.; He, S.; Lin, H.; Wang, C. Platoon Formation Control With Prescribed Performance Guarantees for USVs. *IEEE Trans. Ind. Electron.* **2018**, *65*, 4237–4246. [[CrossRef](#)]
31. Peng, Z.; Wang, D.; Li, T.; Han, M. Output-Feedback Cooperative Formation Maneuvering of Autonomous Surface Vehicles With Connectivity Preservation and Collision Avoidance. *IEEE Trans. Cybern.* **2020**, *50*, 2527–2535. [[CrossRef](#)] [[PubMed](#)]
32. Xue, K.; Wu, T. Distributed Consensus of USVs under Heterogeneous UAV-USV Multi-Agent Systems Cooperative Control Scheme. *J. Mar. Sci. Eng.* **2021**, *9*, 1314. [[CrossRef](#)]
33. Xu, X.; Pan, W.; Huang, Y.; Zhang, W. Dynamic Collision Avoidance Algorithm for Unmanned Surface Vehicles via Layered Artificial Potential Field with Collision Cone. *J. Navig.* **2020**, *73*, 1306–1325. [[CrossRef](#)]
34. Lyu, H.; Yin, Y. COLREGS-constrained real-time path planning for autonomous ships using modified artificial potential fields. *J. Navig.* **2019**, *72*, 588–608. [[CrossRef](#)]
35. Song, J.; Hao, C.; Su, J. Path planning for unmanned surface vehicle based on predictive artificial potential field. *Int. J. Adv. Robot. Syst.* **2020**, *17*, 172988142091846. [[CrossRef](#)]
36. Tan, G.; Zhuang, J.; Zou, J.; Wan, L.; Sun, Z. Artificial potential field-based swarm finding of the unmanned surface vehicles in the dynamic ocean environment. *Int. J. Adv. Robot. Syst.* **2020**, *17*, 172988142092530. [[CrossRef](#)]
37. Sang, H.; You, Y.; Sun, X.; Zhou, Y.; Liu, F. The hybrid path planning algorithm based on improved A* and artificial potential field for unmanned surface vehicle formations. *Ocean Eng.* **2021**, *223*, 108709. [[CrossRef](#)]
38. Chen, F.; Jiang, R.; Zhang, K.; Jiang, B.; Tao, G. Robust backstepping sliding-mode control and observer-based fault estimation for a quadrotor UAV. *IEEE Trans. Ind. Electron.* **2016**, *63*, 5044–5056. [[CrossRef](#)]
39. Song, Y.; He, L.; Zhang, D.; Qian, J.; Fu, J. Neuroadaptive Fault-Tolerant Control of Quadrotor UAVs: A More Affordable Solution. *IEEE Trans. Neural Netw. Learn. Syst.* **2019**, *30*, 1975–1983. [[CrossRef](#)]
40. Park, B.S.; Kwon, J.W.; Kim, H. Neural network-based output feedback control for reference tracking of underactuated surface vessels. *Automatica* **2017**, *77*, 353–359. [[CrossRef](#)]
41. Wen, G.; Chen, C.L.P.; Liu, Y.J. Formation Control With Obstacle Avoidance for a Class of Stochastic Multiagent Systems. *IEEE Trans. Ind. Electron.* **2018**, *65*, 5847–5855. [[CrossRef](#)]
42. Wen, G.; Chen, C.L.P.; Dou, H.; Yang, H.; Liu, C. Formation control with obstacle avoidance of second-order multi-agent systems under directed communication topology. *Sci. China Inf. Sci.* **2019**, *62*, 1–14. [[CrossRef](#)]
43. Shi, Q.; Li, T.; Li, J.; Chen, C.P.; Xiao, Y.; Shan, Q. Adaptive leader-following formation control with collision avoidance for a class of second-order nonlinear multi-agent systems. *Neurocomputing* **2019**, *350*, 282–290. [[CrossRef](#)]
44. Wen, G.; Chen, C.L.P.; Feng, J.; Zhou, N. Optimized Multi-Agent Formation Control Based on an Identifier–Actor–Critic Reinforcement Learning Algorithm. *IEEE Trans. Fuzzy Syst.* **2018**, *26*, 2719–2731. [[CrossRef](#)]
45. Kim, Y.H.; Ahn, S.C.; Kwon, W.H. Computational complexity of general fuzzy logic control and its simplification for a loop controller. *Fuzzy Sets Syst.* **2000**, *111*, 215–224. [[CrossRef](#)]

Disclaimer/Publisher’s Note: The statements, opinions and data contained in all publications are solely those of the individual author(s) and contributor(s) and not of MDPI and/or the editor(s). MDPI and/or the editor(s) disclaim responsibility for any injury to people or property resulting from any ideas, methods, instructions or products referred to in the content.